External seismic pre-isolation retrofit design

J. Giaime, B. Lantz, C. Hardham, R. Adhikari, E. Daw, D. DeBra,
M. Hammond, K. Mason, D. Coyne, D. Shoemaker

April 3, 2002 T020040-00-D

Contents

1 Introduction

This technical note outlines the design of an external seismic pre-isolation system proposed for use in LIGO Livingston. The goal is to reduce the effects of the site's excess ground noise in the 1 - 3 Hz frequency band, allowing detector noise performance equivalent to that of the 4 km LIGO Hanford detector.

The center histogram in Figure 8 shows the most troubling aspect of the excess noise quite clearly. The typical 1 - 3 Hz RMS velocity at LHO is about 2×10^{-8} m/s, but at LLO it is typically 10 - 20 times that during the day. This both makes length control servo lock difficult, and requires greater test mass actuation that adds noise in the gravitational-wave band. In addition, Figure 9 shows that peak velocities in at LLO in the 1 - 3 Hz band are often as large as 2 - 5 μm/s. In order to achieve the promised detector performance at LLO, we are considering proceeding with the rapid development, testing, and installation of an additional stage of seismic isolation, shown in Figure 1. This stage would physically support

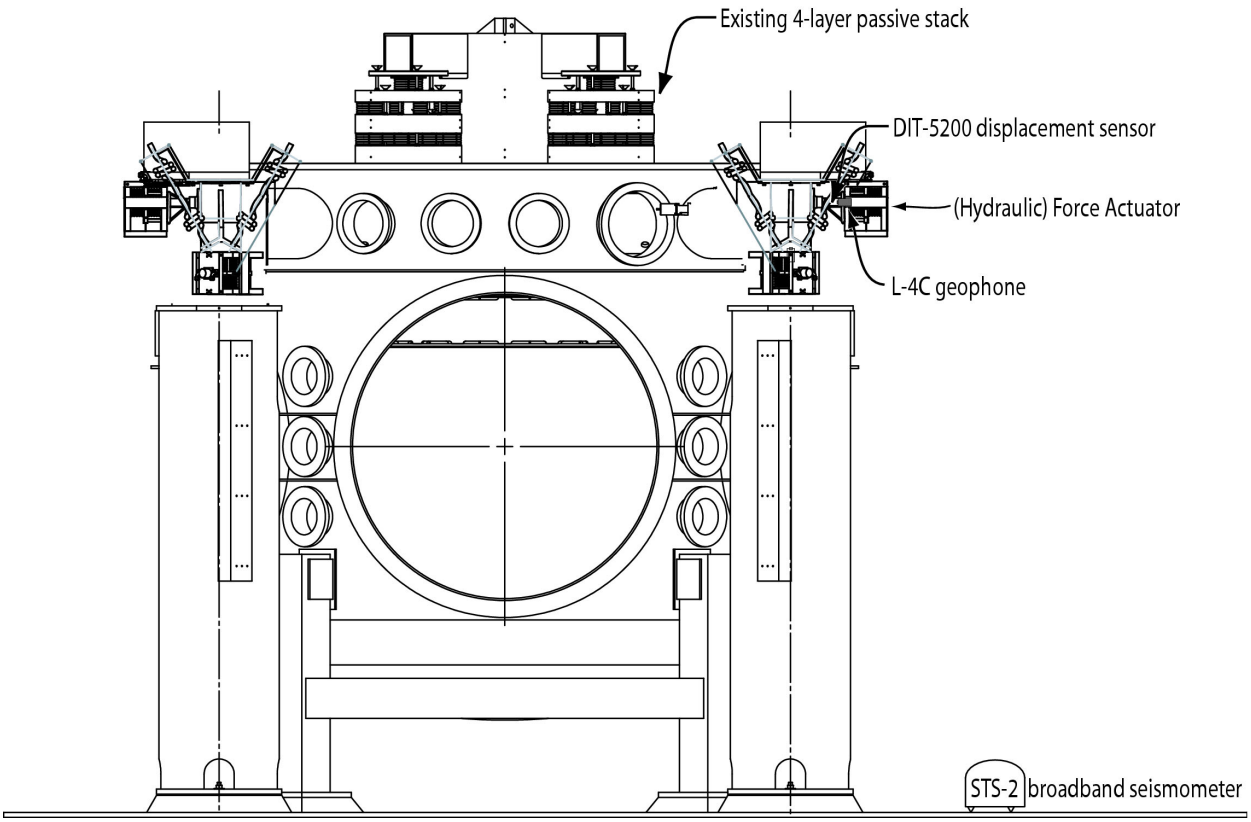

Figure 1: Elevation sketch of a BSC seismic isolation system, with its passive stack payload, external hydraulic actuators, and sensors. The pier-top sensor/actuator package is to be installed on each of the four corners, providing some redundancy on the system's 6 DOF's.

and actively reduce the mechanical noise in the external seismic isolation support structure, replacing the currently installed coarse and fine actuation systems.

Reference [1] lists in detail the requirements for the upgrade under consideration here. (The upgrade is very similar to a stage already under development for Advanced LIGO [5, 6], intended to meet the Advanced LIGO seismic isolation requirements set out in [8].)

2 Active seismic isolation

Active vibration reduction in 6 DOF's has been demonstrated using several techniques. In general, one can measure both the payload's motion and the disturbance (*e. g.,* the floor motion), and use that information to servo the platform's position to that desired by a global commanded position, itself perhaps based on other vibration measurements or the interferometer state. Figure 2 can help explain the relationships among the feedback, feed-forward, and sensor correction techniques. We intend to use all three in this retro-fit design.

Feedback: Environmental noise, which can come in the form of ground noise, acoustic noise, or even temperature, couples into the system's output y through the dynamics in G_d.

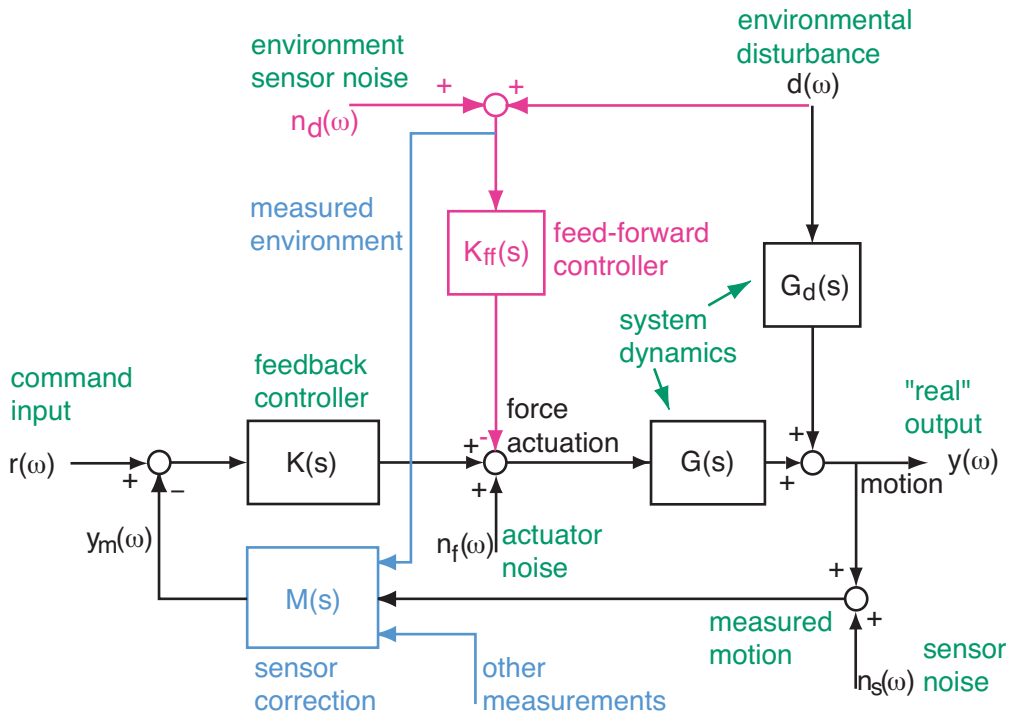

Figure 2: System-level "generic" diagram of the control signal flow within an external vibration reduction system. This includes the controller functions, mechanical dynamics, sensing and actuation, all presumed to be 6 DOF. The places where noise and environmental disturbance influence the system are indicated.

We wish to control y to follow the commanded r, and close a feedback loop. y is measured with a sensor that adds noise n_s; this measured value is subtracted from the desired value r, multiplied by the control law K, and applied as a force (with added noise n_f) to the system, which responds with dynamic function G to give its output, the system's remaining motion. With only feedback, the output can be described by the equation,

$$\begin{aligned} y \;=\; & (I+GK)^{-1}GK\,r && \text{command tracking} \\ & +(I+GK)^{-1}G_d\,d && \text{disturbance suppression} \\ & -(I+GK)^{-1}GK\,n_s && \text{sensor noise} \\ & +(I+GK)^{-1}G\,n_f, && \text{force actuator noise} \end{aligned}$$

where I is the identity matrix for however many DOF's are being controlled. The addition of feedback gain in K suppresses the environmental noise d from the output. If K is sufficiently high, the system tracks r down to a noise floor set by n_s.

Feed-forward: If $K_{ff}G = G_d$, then the environmental disturbance is removed from the system. In practice, this technique is limited by the sensor noise n_d, since the sensor signal must usually be bandpass filtered to avoid introducing excess noise in frequencies where the sensor is not effective. (This filtering can introduce extra phase shifts that prevent perfect

cancellation, which is not reflected in the equation above). While it is true that feedback gain reduces the value at y resulting from the feed-forward correction path by $(I + GK)^{-1}$, the environmental disturbance coupling through K_d is reduced by the same factor, making feed-forward effective regardless of the feedback scheme.

Sensor correction: When a particular sensor's output is corrupted by either environmental noise or unwanted DOF's, the block M can be used to subtract off these things, leaving a "best guess" measurement for use in the feedback path. Two examples of this corruption can be seen in our system, ground motion coupling into the relative position sensors by shaking the SEI piers, and the pitch or yaw DOF's being sensed at low frequencies as horizontal motion in the seismometers. Each of these can at least partially be corrected. In the case of position sensor correction, we can measure the floor motion with a seismometer to provide the correction signal.

Sensor correction differs fundamentally from feed-forward in that it does nothing to the system unless the feedback loop is active. Badly implemented sensor correction can also destabilize the feedback control; feed-forward, done badly, just adds noise.

3 External seismic pre-isolation strategy

3.1 System overview

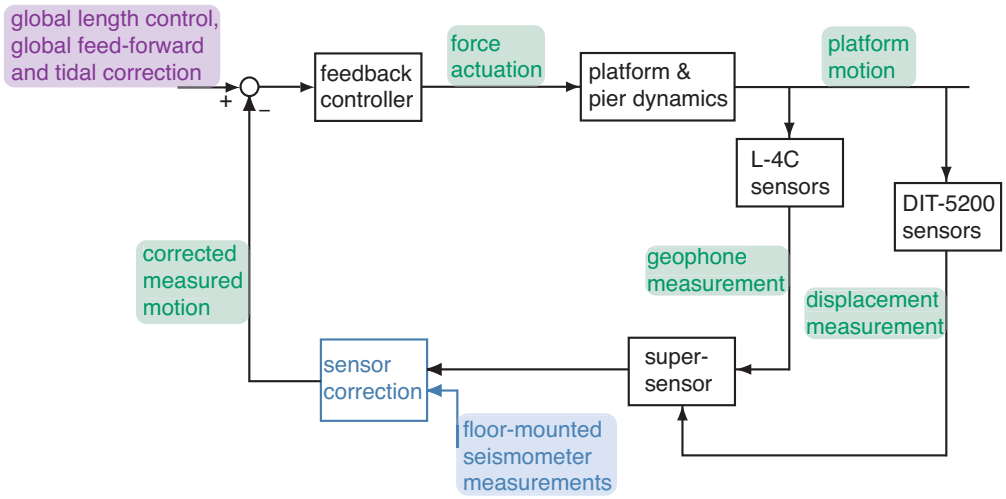

Figure 3: More detailed diagram of the *local* control loop portion of Figure 2, showing where various sensor signals are employed. At left, in purple, the servo is commanded to follow global interferometer length signals and feed-forward correcting signals. The blue sensor correction signal, derived from local seismometer measurements, is used to (for example) correct the relative displacement sensor for the known motion of the local floor.

We plan to use the sensors and actuators shown in Figure 1 to implement feedback and feed-forward in a 6-DOF servo of the external seismic isolation system crossbeam displace-

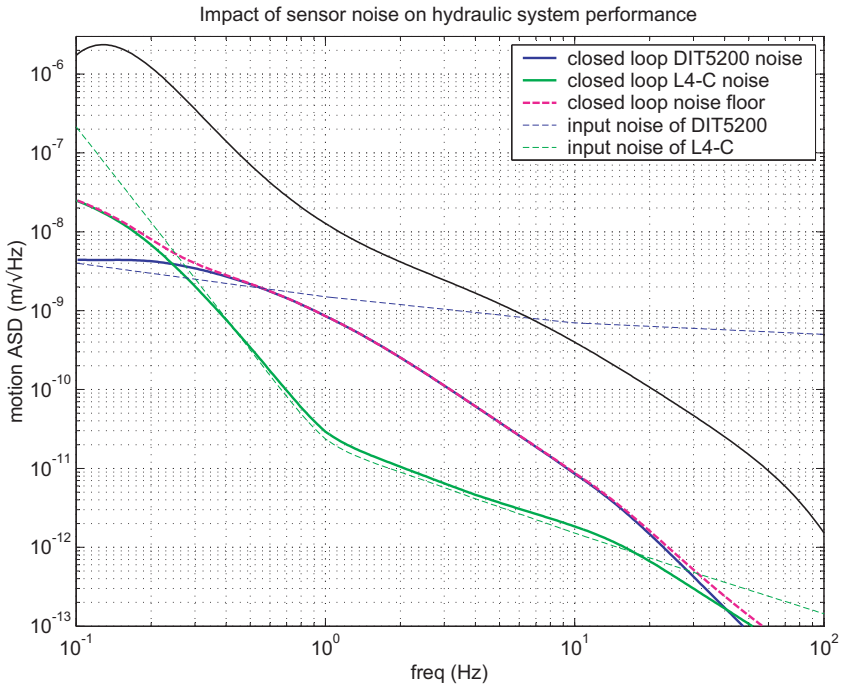

Figure 4: Modelled sensor-originated noise levels in external seismic pre-isolation.

ment. Each existing coarse actuation system and fine actuation system is to be removed. The seismic crossbeam will be supported by a new stiff-spring suspension assembly and actuated by a vertical and tangential hydraulic force-bridge at each pier [2]. (Or, as a backup if the hydraulic device cannot be made to work, an electromagnetic actuator [3].) Figure 3 is a diagram of the local control system. Signals from the 8 local relative displacement sensors, measuring the extension of each of the actuators, and from the 8 geophones mounted in the moving (payload) part of the actuator, are combined in the form of a 8-DOF "super-sensor." The part of the super-sensor that comes from relative displacement sensors is corrected (in at least 3 of its DOF's) for the STS-2 seismometer measured motion of the local floor. This "corrected measured motion," is used to calculate error signals for the 8 local loops. The (corrected) displacement sensors dominate the error functions at low frequencies ($f \lesssim 0.5$ Hz), augmented by the (already implemented) microseism feed-forward and Earth-tidal correction in the laser beam direction. Since most of the troublesome test mass velocity observed at LLO occurs at the stack's 1.2 and 2.1 Hz resonances (see Figure 6), we expect to enhance the loop gain in the geophone at those frequencies in the blend to form the super-sensor. We expect an upper unity gain frequency the super-sensor loop of about 20 Hz.

The impact of sensor noise on the system performance can be seen in Figure 4. This was calculated using a 1-D model of a servo loop with two sensors, one actuator, and an upper unity gain frequency of 20 Hz. This calculation assumes a well behaved plant with no cross-coupling, which allows plant dynamics to be completely ignored. The sensors are the Sercel L-4C 1 Hz geophone readout by a LT1001, and a Kaman DIT-5200 displacement sensor. The input referred noise for the L-4C is calculated based on geophone characteristics and the noise of the LT1001. The input referred noise for the DIT-5200 is based on measurements

by W. Hua of a sensor 1 mm from the center (*i.e.,* the worst-case location). These sensor noise terms are shown as the dashed lines in Fig. 4. The two sensors are blended at 0.5 Hz using reasonable blending filters. The input noise of the sensors appears as the input noise times the forward loop divided by 1 plus the loop gain. The closed loop noise curves are shown as the solid lines. The two noise terms are then added in quadrature to show the impact of sensor noise on the instrument performance (the dashed magenta curve). It is interesting to note that well above 0.5 Hz, even though the main signal for the loop comes from the geophone, the noise is dominated by the displacement sensor, due to its relatively large noise and the conservative nature of the blending used.

The design of the 6-DOF servo loops has not been completed, so we rely on past experience in modelling and testing 6-DOF systems for confidence that stability can be obtained [5, 9, 10, 12]. We expect the geophone inertial servo to provide about a factor of -15 dB in vibration transmission in the 1 - 3 Hz band, enhanced by another factor of a few by targetted resonant gain at the troublesome stack modes. In addition, sensor correction from the floor-mounted STS-2 is expected to give a similar reduction. The latter technique has been tried in a hydraulic test stand at Stanford [2, 6], with performance comparable to what is needed here.

3.2 Low-frequency actuation allocation

Much attention was paid during LIGO's design to avoiding parasitic interferometers between the core optics and non-seismically-isolated structures and optical elements, such as the output optics (see, for example, [13]). A consensus seems to exist that as long as the moving (and light-scattering) object's velocity is less than about 10 μm/s there is less concern about fringe-wrapping effects inserting noise in the GW band.

If we actively or passively quiet the core optics to follow inertia, there will be a relative velocity between them and the floor-mounted components corresponding to the ground velocity. Figure 8 tells the unhappy story that there is from time to time RMS ground velocity $\gtrsim 1$ μm/s in *each* of the frequency bands monitored. Because of this, both the LSC feedback to the test masses and the feed-forward correction for the DF microseismic peak are largely actuated in the ETM's. Other than the extremely small fraction of light ($\approx 10^{-5}$ in intensity) transmitted through the ETM's, no beams exit the ETM tanks. So the fairly large relative motion between each ETM and the adjoining vacuum equipment and lab is less likely to produce parasitic interferometers.

Our baseline design for the external pre-isolation retrofit calls for noise reduction locally at each tank, including the ITM's, with the possible exception of the microseismic correction, which will probably continue to be applied only at the ends. The retrofit system will be identical for all BSC tanks to allow operational flexibility in this. If the parasitic interferometer noise effect becomes a problem, one solution may be to put the external optics tables on seismic isolation mounts.

4 Proof-of-principle tests

4.1 2-DOF external seismic pre-isolation of a BSC SEI

As a test of external actuation, the existing fine actuators were used to close two SISO active seismic isolation loops on LLO's Y-end BSC, as is shown in Figure 5.

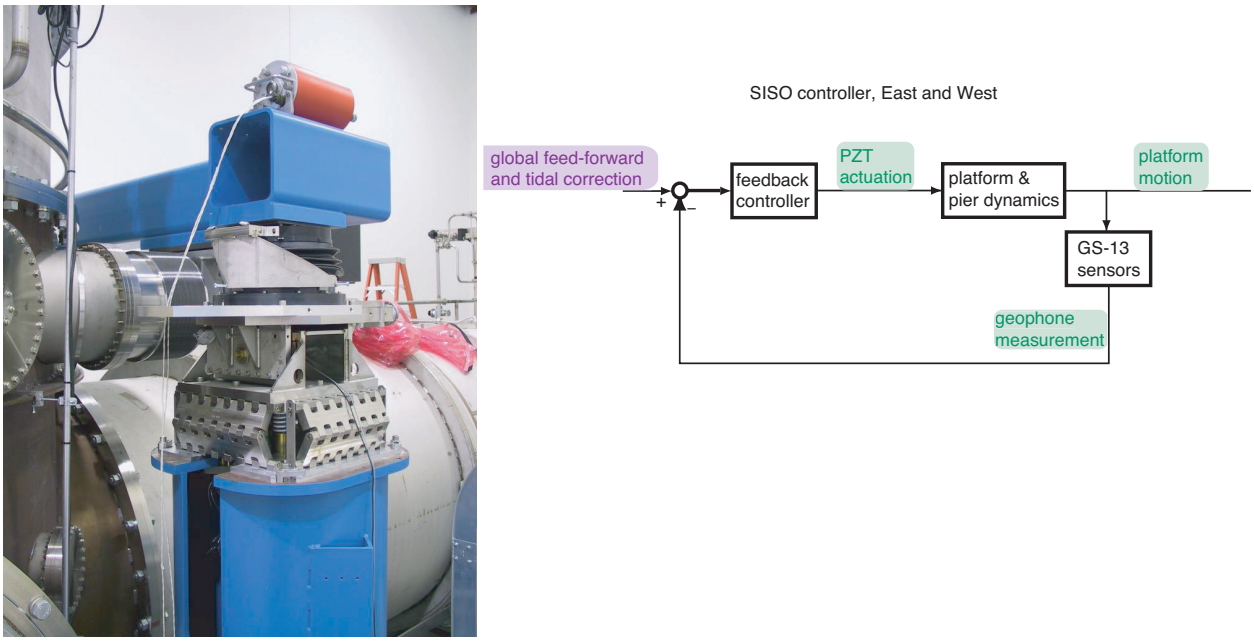

Figure 5: Component setup for proof-of-principle test of external pre-isolation, together with servo diagram.

We placed GS-13 geophones on the east and west sides of the northern cross beam, and used each filtered output as an error signal for an actuator pair. The existing fine actuation system employs a PZT stack whose length is controlled by a drive voltage as part of a PID servo based on an error signal from a colinear strain gauge. We added our geophone-derived error signal at the summing node of the PZT servo. This is topologically very similar to the super-sensor blend that is planned for the retrofit. By using two SISO loops, we were able to avoid instability due to the observed strong coupling to the stack's 6 Hz yaw mode.

We found a very stable loop design having a lower unity gain frequency of about 0.7 Hz. (This is actually a blending point, to the strain-gauge-dominated low frequencies.) The upper UGF is about 7 Hz, and about 10 dB of active noise reduction was obtained in this band. In addition, two resonant gain filters were inserted, allowing the performance seen in Figure 6, measured by monitoring the test mass position with respect to its frame. Figure 7 shows the reduced control signal needed to maintain lock in the Y-arm with the end ETM under active isolation. That particular night excitation of the 2.1 Hz stack mode was dominated by the end station, so it is reduced by a factor of 5 rather than the expeced $\sqrt{2}$ that is seen in the 1.2 Hz peak. This system demonstrates that external seismic pre-isolation can work, although in this case only in the beam direction.

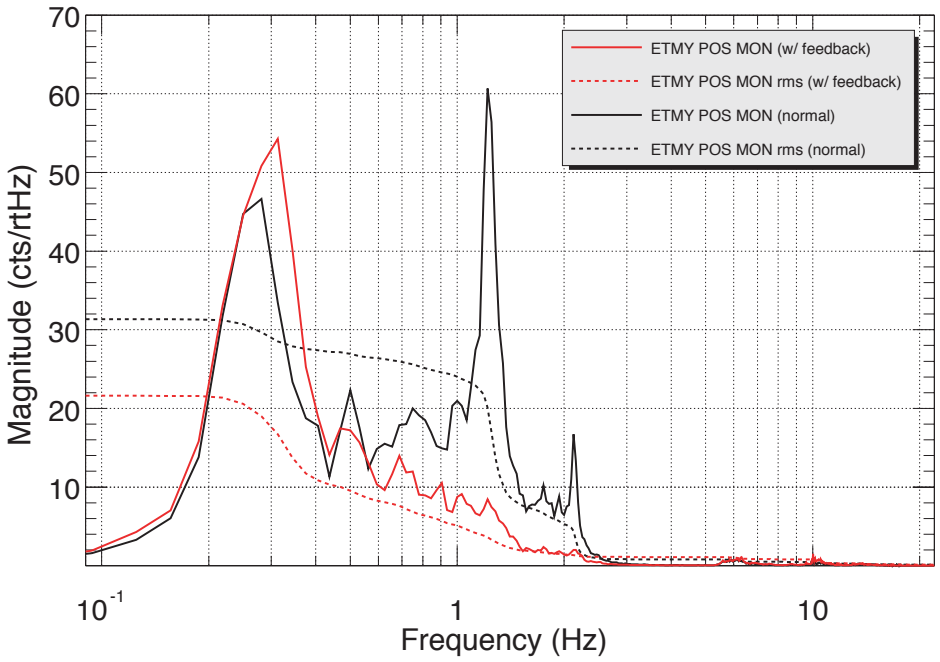

Figure 6: The "POS" output of the ETMY SUS controller, with no global control signals, during a test of 2-DOF external pre-isolation during the evening of March 3, 2002.

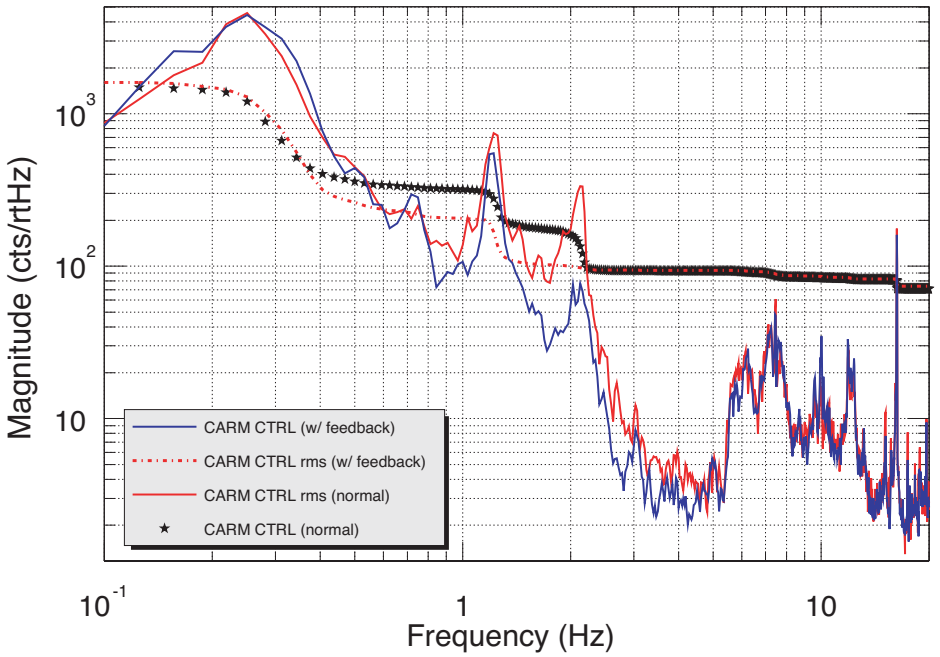

Figure 7: Control signal needed to keep LLO's Y-arm in lock during a test of 2-DOF external pre-isolation during the evening of March 3, 2002.

4.2 2-DOF control using hydraulic actuator prototypes

References [2, 7, 11] describe tests done at Stanford implementing displacement sensor local feedback with sensor correction in two (vertical and horizontal) degrees of freedom. This was carried out using a prototype hydraulic actuator on a test stand holding a spring-suspended realistically-heavy payload.

5 LLO Noise measurements

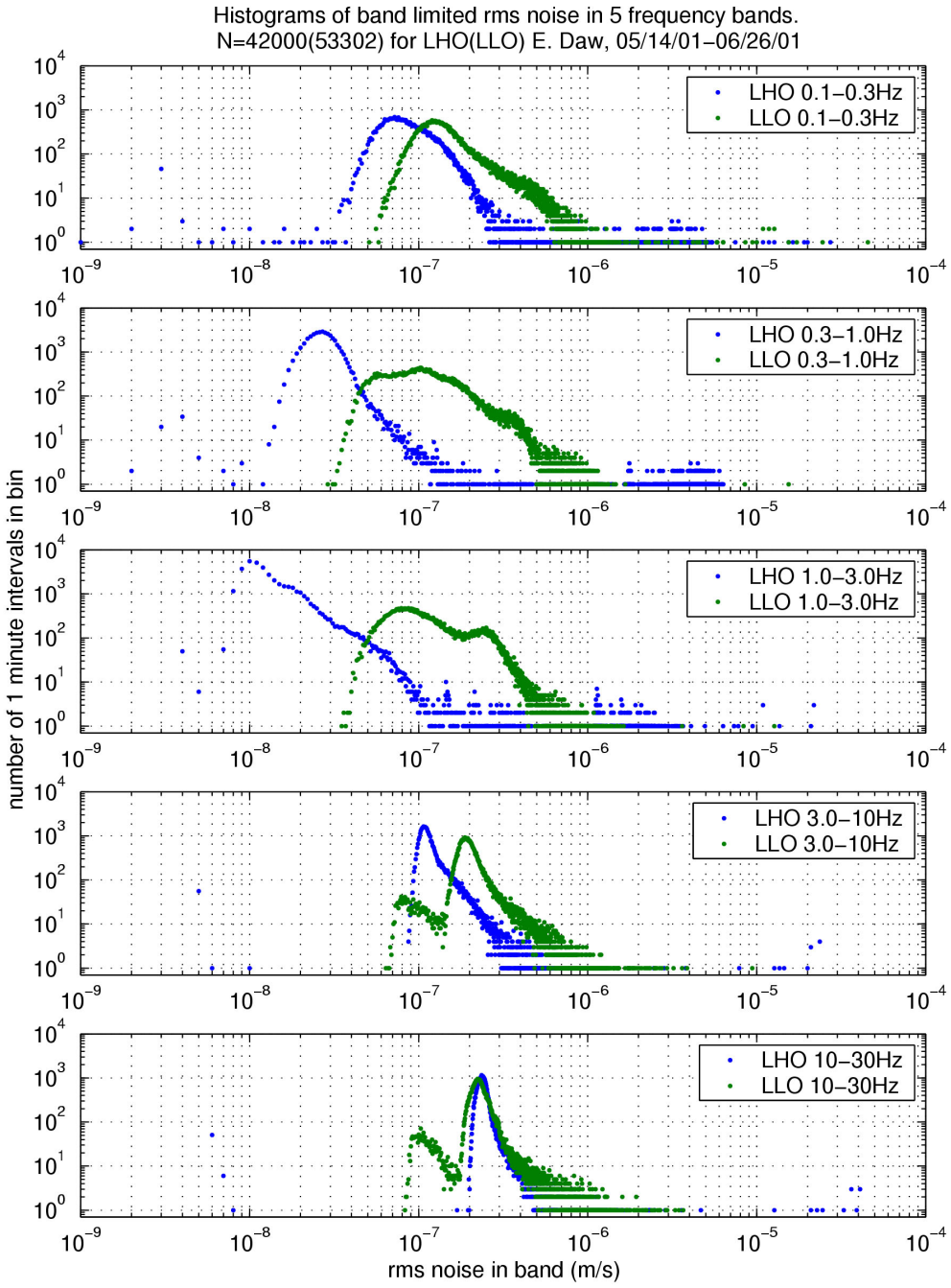

Figure 8: Histograms of the root-mean-squared ground velocity (in m/s) at the two LIGO observatory sites in five frequency bins over 40 days. RMS values above 2 μm/s in the 1 - 3 Hz band are rare. Also note that velocities approaching and exceeding 1 μm/s occur in *every* band shown, at both sites.

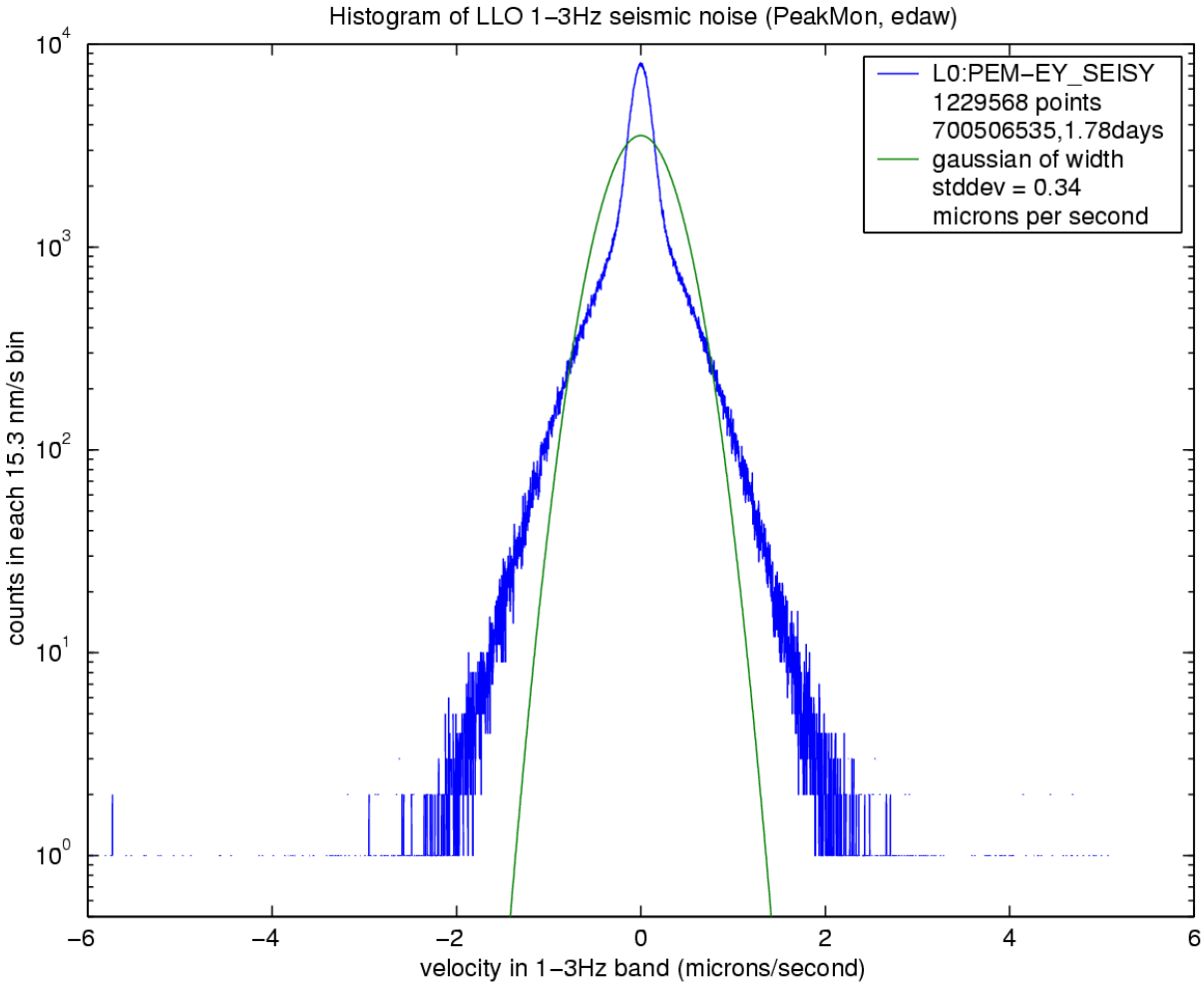

Figure 9: Histogram of the *peak* velocities of 1 - 3 Hz band-limited ground vibration data at LLO, produced by Ed Daw. The data apparently fall into two distributions, probably night/weekend (the narrow central peak), and daytime. Even the latter, and the cause of LLO's difficulties, only very rarely has events greater than 2 μm/s. None were seen greater than about 5 μm/s during this 40-hour data set. We plan on continuous monitoring of this at LLO to gather more statistics.

References

[1] B. Lantz, J. Giaime, P. Fritschel, R. Weiss, D. Coyne, D. Shoemaker, "Initial LIGO Seismic Isolation Upgrade Design Requirements Document." 3/7/02. LIGO-T020033-01-D.

[2] B. Lantz, and others, "Quiet Hydraulic Actuators for Initial LIGO." LIGO-T020047-00-D.

[3] D. Shoemaker, ed., "Pre-Isolator with Electromagnetic Actuator: Conceptual Design, Test Plan." LIGO-T020041-00-D.

[4] D. Coyne, ed., "Initial LIGO Seismic Isolation Upgrade: Conceptual Design Document." LIGO-T020050-00-D.

[5] J. Giaime, B. Lantz, C. Hardham, W. Hua, R. Adhikari, D. Debra, G. Hammond, J. Hammond, J. How, S. Richman, J. Rollins, G. Stapfer, R. Stebbins, "Advanced LIGO Seismic Isolation System Conceptual Design." 1/20/01. LIGO-E010016-00-D.

[6] R Abbott, R Adhikari, G Allen, S Cowley, E Daw, D DeBra, J Giaime, G Hammond, M Hammond, C Hardham, J How, W Hua, W Johnson, B Lantz, K Mason, R Mittleman, J Nichol, S Richman, J Rollins, D Shoemaker,G Stapfer and R Stebbins, "Seismic Isolation for Advanced LIGO," *Class. Quantum Grav.* **19** 1591-1597. (7 April 2002)

[7] J. Giaime, B. Lantz, S. Richman, D. Debra, C. Hardham, J. How, and W. Hua, "Baseline LIGO-II implementation design description of the stiff active seismic isolation system." 3/8/2000. LIGO-T000024-00-U

[8] P. Fritschel, D. Coyne, J. Giaime, B. Lantz, D. Shoemaker, "Seismic Isolation Subsystem Design Requirements Document." 1/17/2001 LIGO-E990303-03-D

[9] Brian Lantz, Wensheng Hua, Sam Richman, Jonathan How, "Computer Modeling and Simulation in Support of the Stiff-Suspension Active Seismic Isolation for LIGO II," 2/14/2000, LIGO T000016-01

[10] Wensheng Hua, Brian Lantz, Sam Richman, "How to construct mechanical model of a mass-spring system," `http://lsuligo.phys.lsu.edu/active/pen3.pdf`

[11] B. Lantz, R. Stebbins, C. Hardham, J. Giaime, "The experimental program in support of stiff-suspension active seismic isolation for LIGO-II," 2/14/2000, LIGO T000015-00.

[12] Richman, S.J.; Giaime, J.A.; Newell, D.B.; Stebbins, R.T.; Bender, P.L.; Faller, J.E.; "Multi-stage active vibration isolation system," Review of Scientific Instruments, **69:6**, 2531. (June '98)

[13] Smith, M., "Up-Conversion of Scattered Light Phase Noise from Large Amplitude Motions" LIGO-T980101-00-D.

[14] Hong Sang Bae, "Active Vibration Isolation and Alignment Issues for LIGO," Masters Thesis, Department of Mechanical Engineering, Stanford University, August 1999.